Structural and Functional Importance of First-Shell Metal Ligands in the Binuclear Manganese Cluster of Arginase I[†,‡]

Evis Cama,[§] Frances A. Emig,[||] David E. Ash,*[,||] and David W. Christianson*[,§]

Roy and Diana Vagelos Laboratories, Department of Chemistry, University of Pennsylvania, Philadelphia, Pennsylvania 19104-6323, and Department of Biochemistry, Temple University School of Medicine, Philadelphia, Pennsylvania 19140

Received March 24, 2003; Revised Manuscript Received May 5, 2003

ABSTRACT: Arginase is a binuclear manganese metalloenzyme that hydrolyzes L-arginine to form L-ornithine and urea. The three-dimensional structures of D128E, D128N, D232A, D232C, D234E, H101N, and H101E arginases I have been determined by X-ray crystallographic methods to elucidate the roles of the first-shell metal ligands in the stability and catalytic activity of the enzyme. This work represents the first structure-based dissection of the binuclear manganese cluster using site-directed mutagenesis and X-ray crystallography. Substitution of the metal ligands compromises the catalytic activity of the enzyme, either by the loss or disruption of the metal cluster or the nucleophilic metal-bridging hydroxide ion. However, the substitution of the metal ligands or the reduction of $Mn^{2+}{}_A$ or $Mn^{2+}{}_B$ occupancy does not compromise enzyme−substrate affinity as reflected by K_M, which remains relatively invariant across this series of arginase variants. This implicates a nonmetal binding site for substrate L-arginine in the precatalytic Michaelis complex, as proposed based on analysis of the native enzyme structure (Kanyo, Z. F., Scolnick, L. R., Ash, D. E., and Christianson, D. W. (1996) *Nature 383*, 554−557).

Rat arginase I is a 105 kDa homotrimer that catalyzes the hydrolysis of L-arginine to form L-ornithine and urea (*1*−*3*):

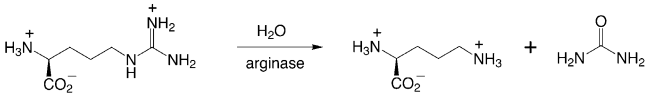

The crystal structure of rat arginase I reveals a binuclear manganese cluster ($Mn^{2+}{}_A$−$Mn^{2+}{}_B$ separation = 3.3 Å) at the base of a 15 Å-deep active site cleft, with $Mn^{2+}{}_A$ being more deeply situated (*4*). The $Mn^{2+}{}_A$ ion is coordinated by H101 (Nδ), D124 (Oδ1), D128 (Oδ1), and D232 (Oδ1), and $Mn^{2+}{}_B$ is coordinated by H126 (Nδ), D124 (Oδ2), D232 (Oδ1), and D234 (Oδ1 and Oδ2); a solvent molecule symmetrically bridges $Mn^{2+}{}_A$ and $Mn^{2+}{}_B$ and donates a hydrogen bond to Oδ2 of D128 (Figure 1). Although arginase I is localized predominantly in mammalian liver where it catalyzes the final cytosolic step of the urea cycle, a second mammalian isozyme, arginase II, is localized in nonhepatic tissues where it functions primarily in L-arginine homeostasis (*1*−*3*).

An intact binuclear metal cluster is required for maximal catalysis by arginase I (*5*). It is generally accepted that catalysis proceeds via a metal-activated hydroxide mechanism in which both $Mn^{2+}{}_A$ and $Mn^{2+}{}_B$ serve to polarize and orient a bridging hydroxide ion for nucleophilic attack at the scissile guanidinium carbon of the substrate, which in turn is held in place by hydrogen bond interactions with E277 and the backbone carbonyl of H141 (*4*, *6*, *7*):

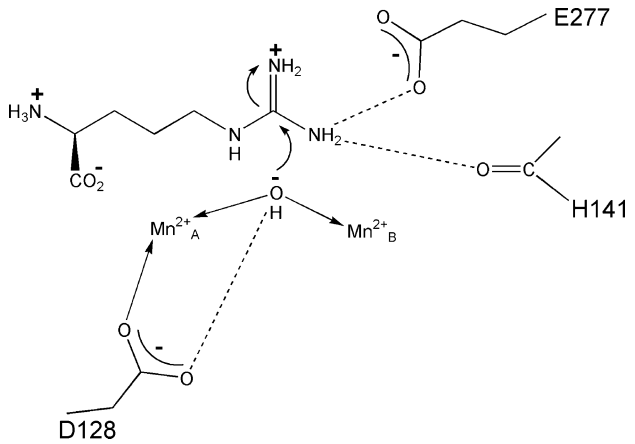

An alternative mechanism is proposed in which the substrate L-arginine coordinates to $Mn^{2+}{}_B$, and $Mn^{2+}{}_A$ polarizes the nucleophilic solvent molecule (*8*), but enzyme−substrate interactions proposed in this model are inconsistent with the three-dimensional structure of the active site: for

[†] This work was supported by Grants GM49758 (D.W.C.) and GM67788 (D.E.A.) from the National Institutes of Health. E.C. was supported in part by the U.S. Army Medical Research and Materiel Command's Office of the Congressionally Directed Medical Research Programs through a Department of Defense Breast Cancer Research Predoctoral Fellowship.

[‡] The atomic coordinates and structure factors for arginase I variants have been deposited in the Protein Data Bank, www.rcsb.org, with accession codes 1P8R (H101E), 1P8P (H101N), 1P8N (D232A), 1P8S (D232C), 1P8M (D128E), 1P8O (D128N), and 1P8Q (D234E).

* To whom correspondence should be addressed. E-mail: (D.W.C.) chris@xtal.chem.upenn.edu; (D.E.A.) deash@temple.edu.

[§] University of Pennsylvania.

[||] Temple University.

10.1021/bi030074y CCC: $25.00
Published on Web 06/06/2003

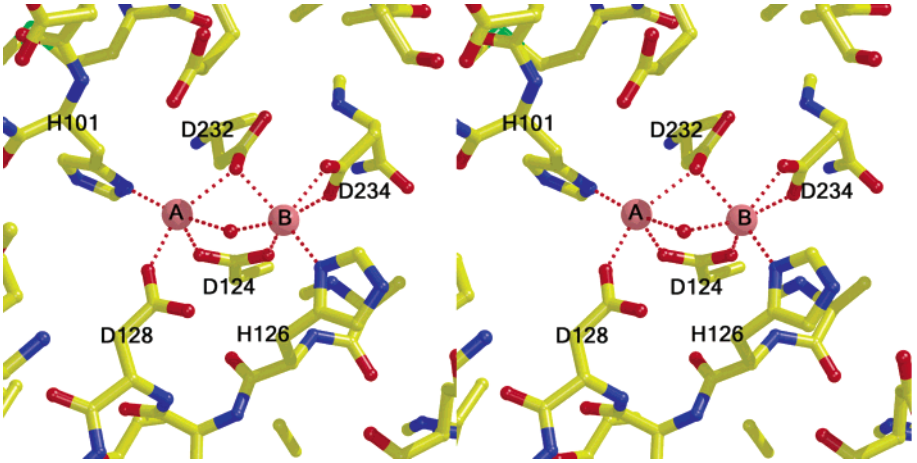

FIGURE 1: Binuclear manganese cluster of native arginase. The coordination geometry of Mn^{2+}_A is square pyramidal, and that of Mn^{2+}_B is distorted octahedral. The Mn^{2+}_A−Mn^{2+}_B separation is 3.3 Å. The metal-bridging hydroxide ion appears as a red sphere.

Table 1: Primers Used in Site-Directed Mutagenesis[a]

mutant	primer in forward direction
D232A	GGCCCATTCACCTGAGTTTTGCTGTTGATGGACTGGACCCAG
D232C	GGCCCATTCACCTGAGTTTTTGCGTTGATGGACTGGACCCAG
D128E	GGGTGGATGCTCACACTGAAATCAACACTCCGCTGACAACC
D128N	GGGTGGATGCTCACACTAACATCAACACTCCGCTGACAACC
D234E	CACCTGAGTTTTGATGTTGAAGGACTGGACCCAGTATTCACC
H101E	GTGGTGCTGGGTGGAGACGAAAGTATGGCAATTGGAAGCATC
mutant	**primer in reverse direction**
D232A	CTGGGTCCAGTCCATCAACAGCAAAACTCAGGTGAATGGGCC
D232C	CTGGGTCCAGTCCATCAACGCAAAAACTCAGGTGAATGGGCC
D128E	GGTTGTCAGCGGAGTGTTGATTTCAGTGTGAGCATCCACCC
D128N	GGTTGTCAGCGGAGTGTTGATGTTAGTGTGAGCATCCACCC
D234E	GGTGAATACTGGGTCCAGTCCTTCAACATCAAAACTCAGGTG
H101E	GATGCTTCCAATTGCCATACTTTCGTCTCCACCCAGCACCAC

[a] Mutated bases are underlined.

example, the proposed substrate Nϵ-H···E277 hydrogen bond (*8*) is geometrically inconsistent with the binding of boronic acid substrate analogues (*6*, *7*). Moreover, measurements of kinetic constants for arginase I variants reveal an invariant K_M despite perturbations in the binuclear manganese cluster, including extraction of Mn^{2+}_A (*9*, *10*), consistent with a nonmetal binding site for L-arginine in the Michaelis complex.

Given the importance of an intact binuclear manganese cluster for catalysis, the first-shell metal ligands must play an important role in stabilizing this cluster with the proper geometry for optimal catalysis. Additionally, the recently determined structures of arginases I and II complexed with a reactive boronic acid substrate analogue bound as an analogue of the tetrahedral intermediate suggest that coordination changes may occur upon the formation of this intermediate in catalysis: specifically, Oδ1 of D232 may weaken its coordination with Mn^{2+}_B to hydrogen bond with the η_2-NH_2 group of the substrate and/or tetrahedral intermediate (*7*, *11*). Therefore, modest pliability appears to be important in the metal coordination polyhedra to accommodate the complete reaction coordinate of catalysis.

To probe the function of first-shell metal ligands in the binuclear manganese cluster of arginase I, we have determined the X-ray crystal structures of the H101E, D128N, D128E, D232A, and D234E variants, and we have re-refined the structure of the H101N variant. This work reveals significant structure−stability relationships for the metal cluster and also highlights important structure−mechanism relationships pertaining to the role of the intact cluster in catalysis.

MATERIALS AND METHODS

Mutagenesis and Protein Preparation. In vitro site-directed mutagenesis was performed using the QuikChange kit from Stratagene. Forward and reverse primers were constructed for each of the mutations as listed in Table 1. Recombinant rat liver arginase cDNA expressed in *Escherichia coli* with a pET29 T7-based expression vector (Novagen) was used as a template for these mutations. The PCR[1] mutant construct products were used to transform BL21-Gold (DE3) competent cells. These cells were then plated on kanamycin agar plates, and plasmid DNA for each of the mutants was isolated from the resulting colonies. The plasmid DNA was isolated using a Qiagen kit, and the DNA was digested using *BamH1* and *NdeI* restriction enzymes known to have unique restriction sites located outside of the arginase cDNA. Positive

[1] Abbreviations: ABH, (*S*)-2-amino-6-boronohexanoic acid; BEC, *S*-(2-boronoethyl)-L-cysteine; CHES, 2-(*N*-cyclohexylamino)-ethanesulfonic acid; EDTA, ethylenediaminetetraacetic acid; HEPES, *N*-(2-hydroxyethyl)-piperazine-*N*-2-ethanesulfonic acid; IPTG, isopropyl β-D-1-thiogalactopyranoside; LB, Lennox L broth; PEG, poly(ethylene glycol); PMSF, phenylmethanesulfonyl fluoride; PCR, polymerase chain reaction; EPR, electron paramagnetic resonance.

constructs were identified by this restriction mapping and were sent for DNA sequencing to the University of Pennsylvania DNA Sequencing Facility. The DNA sequence for each of the constructs was checked to verify that only the desired mutation was made and no other mutations were introduced during the PCR reaction.

Mutant constructs identified as positive for the desired mutation and containing no other mutations were used to transform BL21-Gold (DE3) cells. One positive colony for each of the mutants was grown overnight in 250 mL of LB media containing 30 μg/mL kanamycin at 37 °C. Cells from this culture were used to inoculate 6 L of LB media containing 30 μg/mL kanamycin. These cultures were grown at 37 °C until they reached an A_{600} of 0.8 and then were induced with 0.2 mg/mL IPTG. The induced cells were shaken for 3 h at 37 °C, after which they were harvested by centrifugation at 5000*g* for 30 min. Cells were stored at −80 °C.

As needed, cells were thawed at 37 °C for 1 h and resuspended in 50 mM HEPES-KOH (pH 7.5), 1 mM PMSF, 1 mM EDTA, and a final concentration of 1 mg/mL lysozyme. Arginase I variants were purified according to the method described by Cavalli and co-workers (*9*). Briefly, cells were sonicated and after centrifugation, $MnCl_2$ was added to the supernatant at a final concentration of 20 mM. The supernatant was placed in a 60 °C water bath for 30 min and subsequently centrifuged at 20 000*g* for 30 min. Ammonium sulfate was added to the supernatant to 85% saturation, and following centrifugation the pellet was resuspended in 50 mM HEPES-KOH (pH 7.5). The supernatant was dialyzed exhaustively, centrifuged at 20 000*g* for 31 min, applied to a Sigma Reactive Red column, and eluted with a 0.0−0.3 M linear gradient of KCl in 50 mM HEPES-KOH (pH 7.5). Protein-containing fractions were collected, and the purity was assessed by SDS−PAGE with the protein concentration determined by a Bradford assay at 595 nm. Arginase I variants were stored at 4 °C in 85% ammonium sulfate.

Enzyme Assays. Arginase I variants were assayed for arginase activity using the method of Rüegg and Russell (*12*) with the following modifications: enzyme variants were resuspended in 50 mM HEPES-KOH (pH 7.5), $MnCl_2$ was added to a final concentration of 10 mM, and the samples were heat-activated in a 60 °C water bath for 10 min. Samples were then centrifuged at 20 000*g* for 20 min to remove any precipitation, and the supernatant was dialyzed three times with 50 mM HEPES-KOH (pH 7.5).

The reaction mixture used to perform the kinetic assays contained 100 mM CHES-NaOH (pH 9.0), 100 μM $MnCl_2$, and 0.05 μCi of L-[guanidine-^{14}C]arginine in a 40 μL volume per centrifuge tube. A 5 μL volume of increasing nonradiolabeled L-arginine concentrations was added to the reaction mixtures to give final arginine concentrations of 0, 0.5, 1, 2, 3, 4, 5, 10, 15, 20, 25, 40, and 60 mM. Reactions were started by the addition of 5 μL of a 1 μg/mL solution of the enzyme variants and incubated for 5−120 min. The reactions were stopped by the addition of 400 μL of the stop solution containing 0.25 mM acetic acid (pH 4.5), 7 M urea, 10 mM L-arginine, and a 1:1 (v/v) slurry of Dowex W-X8 in water. The reaction mixture was vortexed immediately after the addition of the stop solution, gently mixed for an additional 10 min, and centrifuged at 6000 rpm for 10 min. A 200 μL volume of the supernatant was removed, and 3 mL of scintillation liquid EcoScint was added in preparation for liquid scintillation counter in a Beckman counter.

Electron Paramagnetic Resonance (EPR). Protein variants stored in 85% ammonium sulfate were pelleted by centrifugation at 14 000 rpm for 20 min. Pellets were resuspended in 50 mM HEPES-KOH (pH 7.5), and $MnCl_2$ was added to a final concentration of 10 mM. Protein solutions were then heat-activated in a 60 °C water bath for 10 min. Any resulting precipitate from the heat activation step was removed by centrifugation at 14 000 rpm for 20 min. Supernatants were then dialyzed five times with Chelex-100-treated 50 mM HEPES-KOH (pH 7.5), and the protein solutions were concentrated to about 1−3 mg/mL. A 200 μL volume of each protein solution was mixed with 200 μL of 6% perchloric acid to give a final volume of 400 μL. Manganese standards were prepared in perchloric acid as described for the protein solutions. EPR spectra were recorded at 300 K on a Bruker ER-200D-SRC spectrometer. The manganese content for each arginase I sample was determined by comparison of EPR spectral amplitudes for the enzyme samples with a standard curve generated by plotting spectral amplitude versus manganese concentration for the solutions of known manganese concentrations.

Crystallography. H101E arginase I was crystallized using the hanging drop vapor diffusion method. A 3 μL drop of precipitant solution [0.1 M HEPES-NaOH (pH 7.5), 10% v/v 2-propanol, 20% w/v PEG 4000] was added to a 3 μL drop of protein solution [8−10 mg/mL H101E arginase I, 50 mM bicine-NaOH (pH 8.5), 100 μM $MnCl_2$, 2 mM *S*-(2-boronoethyl)-L-cysteine (BEC)] on a silanized cover slip subsequently inverted and sealed over a 1 mL reservoir of precipitant solution at 4 °C. Crystals grew in 2−3 weeks with approximate dimensions of 0.1 × 0.1 × 0.4 mm^3. Crystals diffracted to 2.5 Å resolution, and deviations from the expected Wilson statistics with $\langle I^2\rangle/\langle I\rangle^2 \approx 1.5$ indicated perfect hemihedral twinning (*13*−*16*). The symmetry of the diffraction pattern was consistent with apparent space group *P*6 and true crystallographic space group *P*3 with a twinning fraction of 0.5 ($a = b = 91.0$ Å, $c = 69.3$ Å; data collection statistics are recorded in Table 2). Crystals of the H101E arginase I−BEC complex were isomorphous with the perfectly twinned crystals formed by the arginase I−BEC complex (*7*) and arginase I−ABH complex (*6*).

The D128E, D128N, D232A, D232C, and D234E arginase I variants were crystallized using the hanging drop vapor diffusion method. Briefly, a 3 μL drop of precipitant solution [50 mM bicine-NaOH (pH 8.2−8.5), 20−30% PEG 8000, 2−5 mM $MnCl_2$] was added to a 3 μL drop of protein solution [10−16 mg/mL arginase I variant, 50 mM bicine-NaOH (pH 8.5), 100 μM $MnCl_2$] on a silanized cover slip subsequently inverted and sealed over a 1 mL reservoir of precipitant buffer at 4 °C. Crystals of these variants appeared after 4 weeks and were nearly isomorphous with those of the wild-type enzyme (*4*). Crystals belonged to space group $P3_2$ with unit cell parameters as follows. D128E: $a = b = 88.5$ Å, $c = 113.9$ Å; D128N: $a = b = 88.5$ Å, $c = 111.5$ Å; D232A: $a = b = 90.3$ Å, $c = 104.9$ Å; D232C: $a = b = 90.9$ Å, $c = 105.7$ Å; and D234E: $a = b = 88.3$ Å, $c = 111.8$ Å. Data collection statistics are recorded in Table 2.

Prior to data collection, crystals were gradually transferred to a cryoprotectant solution consisting of the original

Table 2: Data Collection and Refinement Statistics

	D128E	D128N	D232A	D232C	D234E	H101E-BEC
resolution (Å)	2.84	2.96	2.9	3.2	2.95	2.5
total reflections (*N*)	23974	18329	19140	14992	18830	22138
completeness (%) (last shell)[a]	97.4 (98.2)	93.4 (95.1)	95.7 (98.3)	92.9 (93.9)	95.3 (92.1)	100 (100)
R_{merge} (last shell)[a,b]	0.057 (0.227)	0.087 (0.300)	0.066 (0.411)	0.080 (0.44)	0.075 (0.377)	0.099 (0.328)
reflections used in refinement/test set	22156/1080	16873/869	18307/892	13956/732	17362/845	21905/2051
protein atoms (*N*)[c]	7191	7187	7179	7182	7191	4688
Mn^{2+} ions (*N*)[c]	6	6	3	6	6	6
solvent/ligand atoms (*N*)[c]	42	18	50	32	42	38/26
R_{cryst}[d]	0.286	0.293	0.286	0.286	0.261	0.144
R_{free}[d]	0.2981	0.297	0.305	0.315	0.287	0.201
			rms Deviations			
bonds (Å)	0.015	0.014	0.014	0.011	0.009	0.007
angles (deg)	1.7	1.6	1.7	1.7	1.4	1.4
dihedral angles (deg)	24.4	23.9	23.8	24.0	23.3	23.2
improper dihedral angles (deg)	1.4	1.0	1.4	1.3	1.2	0.9
			Average *B* factors			
protein	74	77	83	85	68	19.5
Mn^{2+} ions	68	60	80	63	97/50	18.5
solvent/ligand atoms	72	55	66	45	40	18/30

[a] Numbers in parentheses refer to the outer 0.1 Å shell of data. [b] R_{merge} for replicate reflections, $R = \sum|I_h - \langle I_h\rangle|/\sum\langle I_h\rangle$; I_h = intensity measured for reflection *h* and $\langle I_h\rangle$ = average intensity for reflection *h* calculated from replicate data. [c] Per asymmetric unit. [d] Crystallographic *R* factor, $R_{cryst} = \sum||F_o| - |F_c||/\sum|F_o|$ for reflections contained in the working set. Free *R* factor, $R_{free} = \sum||F_o| - |F_c||/\sum|F_o|$ for reflections contained in the test set held aside during refinement (5% of total). $|F_o|$ and $|F_c|$ are the observed and calculated structure factor amplitudes, respectively.

precipitant solution plus 30% glycerol and then flash-cooled with liquid nitrogen. X-ray diffraction data for the H101E variant were collected on a MAR 345 mm image plate detector at Stanford Synchrotron Radiation Laboratory (beam line 7-1) at the Stanford Linear Accelerator Center, Menlo Park, CA. X-ray diffraction data for the D128E, D128N, D232C, D232A, and D234E variants were collected at the Cornell High Energy Synchrotron Source (beam line F-1). Intensity data integration and reduction were performed using the HKL suite of programs (*17*).

The wild-type arginase I−BEC complex (*7*) was used as a model for molecular replacement calculations to solve the structure of the twinned H101E arginase I−BEC complex. Structure factor amplitudes for the calculation of electron density maps were generated from deconvoluted intensities using the structure-based detwinning algorithm of Redinbo and Yeates (*16*) in the same manner as utilized for the structure determination of the wild-type arginase I−ABH and arginase I−BEC complexes (*6*, *7*). Iterative rounds of refinement and rebuilding of the native model were performed using the programs CNS (*18*) and O (*19*), respectively. For simultaneous refinement of the H101E−BEC complex in both twin domains against the twinned structure factor amplitudes $|F_o|$ derived from the measured twinned intensities I_o, the target residual was based on the numerator of R_{twin} as implemented in CNS (*18*). In the final stages of refinement, BEC was built into the electron density map. Strict noncrystallographic symmetry was employed at the beginning of the refinement and later relaxed to appropriately weighted constraints as judged by the $R_{twin/free}$.

Initial phases for D128E, D128N, D234E, D232C, and D232A arginases I were determined by molecular replacement with AmoRe (*20*, *21*) using the structure of the rat liver arginase trimer (*4*) (less the atoms of the variant side chain) as a search probe. Strict noncrystallographic symmetry was employed at the beginning of the refinement and relaxed to appropriately weighted constraints as judged by R_{free} as refinement progressed. After initial rounds of refinement, the electron density for the variant side chains was clear and unambiguous in electron density maps generated with Fourier coefficients $2|F_o| - |F_c|$ and $|F_o| - |F_c|$ and phases calculated from the in-progress atomic model. Iterative rounds of refinement and model adjustment were performed using CNS (*18*) and O (*19*), respectively. Individual *B* factors were refined for the D128E, D234E, H101N, and H101E variants, and group *B* factors were refined for the D232A and D232C variants. A bulk solvent correction was applied. Refinement statistics are reported in Table 2. On average, 89% of the residues fall into the most favorable region of the Ramachandran plot, and as in the native enzyme structure, there is only one outlier per monomer (N65). The overall structure of each arginase variant is similar to that of the native enzyme (rms deviations of C_α atoms are 0.120−0.254 Å). Figures were generated using BOBSCRIPT and Raster3D (*22*, *23*).

RESULTS AND DISCUSSION

Analysis of the arginase I and arginase II structures suggests that L-arginine hydrolysis is achieved by a metal-activated hydroxide ion that symmetrically bridges Mn^{2+}_A and Mn^{2+}_B (*4*, *6*, *7*, *11*). Therefore, the precise positioning of the metal cluster is required to stabilize the nucleophilic hydroxide ion in the proper location and orientation for catalysis. Additionally, the metal cluster tunes the reactivity of the nucleophile: to illustrate, the pK_a of water is 15.7, the pK_a of $Mn^{2+}(OH_2)_6$ is 10.6 (*24*), and the ionization of water to yield the metal-bridging hydroxide ion in the arginase I active site is likely responsible for the activity-linked pK_a of 7.9 (*25*).

Overall, amino acid substitutions in the manganese coordination polyhedra of arginase I result in a wide array of compromised metal binding properties and residual catalytic activities (Table 3). Although substrate K_M values vary by no more than 2-fold relative to that measured for the wild-type enzyme, k_{cat} values are depressed from 32-fold to nearly 10^5-fold. As K_M is an indication of enzyme−substrate

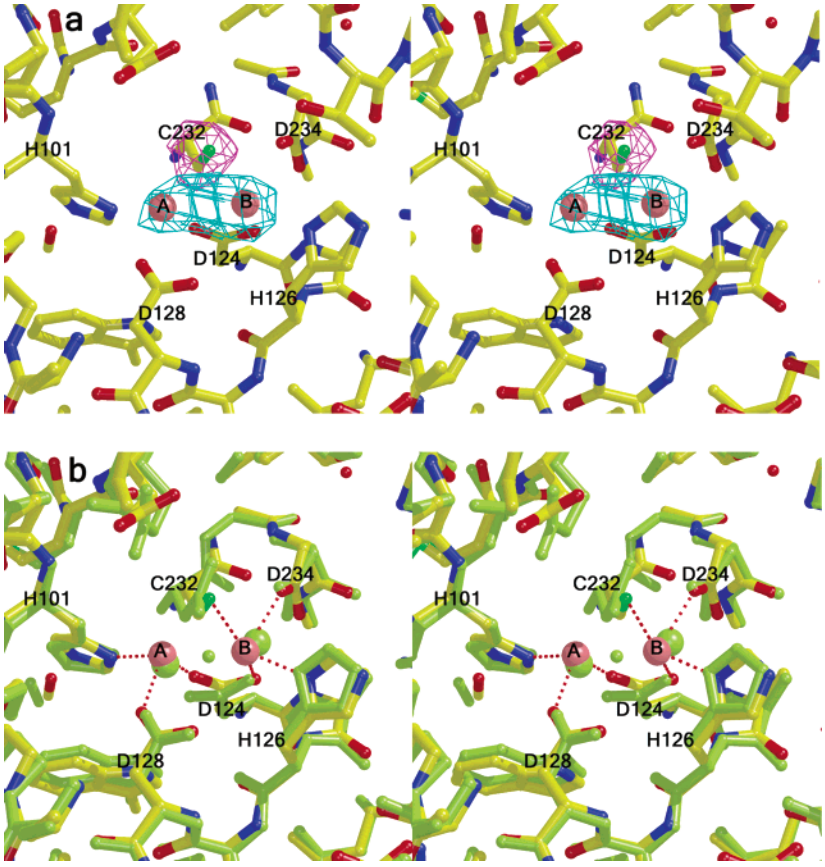

FIGURE 2: D232C arginase I. (a) Simulated annealing omit electron density maps of the binuclear manganese cluster calculated with Fourier coefficients $|F_o| - |F_c|$ less the atoms of C232 (magenta, contoured at 3σ) or $Mn^{2+}{}_A$ and $Mn^{2+}{}_B$ (cyan, contoured at 8.6σ). (b) Manganese coordination interactions (red dashed lines). For reference, the native arginase I structure is superimposed (pale green).

Table 3: Functional Properties of Arginase Variants[a]

variant	K_M (mM)	k_{cat} (s^{-1})	k_{cat}/K_M ($mM^{-1}\,s^{-1}$)	Mn^{2+}:protein stoichiometry (EPR)	Crystallographic occupancy (%)	
					$Mn^{2+}{}_A$	$Mn^{2+}{}_B$
wild-type[b,c]	1.4	250.0	179.0	2.0	100	100
D232A	1.6	0.012	0.007	1.0	100	0
D232C	1.0	1.5	1.5	1.5	100	70
D128E	1.4	0.07	0.05	1.3	80	100
D128N	1.1	0.003	0.003	0.94	50	100
D128A	1.0	0.003	0.003	n.d.	n.d.	n.d.
D234E	2.5	6.6	2.6	1.6	100	50
D234A	2.5	0.4	0.16	1.6	n.d.	n.d.
D234H	2.5	0.2	0.08	1.5	n.d.	n.d.
H101E	2.9	7.7	2.6	n.d.	100	100
H101N[b]	1.0	118.0	118.0	1.1	50[d]	100[d]

[a] n.d., not determined; estimated uncertainties in kinetic, EPR, and crystallographic measurements are ±10%. [b] Ref *9*. [c] Ref *5*. [d] Ref *10* and E.C., unpublished results.

affinity, these data suggest that L-arginine does not coordinate to $Mn^{2+}{}_A$ or $Mn^{2+}{}_B$ prior to catalysis. Insofar that k_{cat} is highly sensitive to an intact binuclear manganese cluster and the reactivity of the metal-bridging hydroxide ion, the structures of these variants are interpreted below in view of the functional data recorded in Table 3.

Structural and Functional Consequences of D232 Substitutions. In the wild-type enzyme, Oδ1 of D232 symmetrically bridges both $Mn^{2+}{}_A$ and $Mn^{2+}{}_B$ (Figure 1) (*4*), and deletion of this ligand in the D232A variant destabilizes $Mn^{2+}{}_B$ binding sufficiently so that only $Mn^{2+}{}_A$ is observed in the active site (data not shown). The $Mn^{2+}{}_A$ ion is coordinated by D128 (Oδ1), H101 (Nδ1), D124 (Oδ1), and a solvent molecule with distorted tetrahedral geometry. Although the $Mn^{2+}{}_A$ position remains unchanged, the remaining aspartate metal ligands undergo slight structural changes to accommodate the D232A substitution and the loss of $Mn^{2+}{}_B$.

In contrast, the D232C variant contains a reasonably intact binuclear manganese cluster: $Mn^{2+}{}_A$ is coordinated by H101 (Nδ1), D128 (Oδ1), and D124 (Oδ1), while $Mn^{2+}{}_B$ is coordinated by H126 (Nδ1), D234 (Oδ2), and D124 (Oδ2); the average $Mn^{2+}{}_A$—$Mn^{2+}{}_B$ separation is 2.9 Å. The coordination of $Mn^{2+}{}_B$ by D234 changes from symmetrically bidentate to monodentate by Oδ2. No metal-bound solvent molecules are observed in the electron density map (Figure 2a), probably because of the modest 3.2 Å resolution of the structure determination. Overall, there are no major structural differences between D232C and native arginases I (Figure 2b).

The Sγ atom of the engineered C232 side chain is 3.0 Å from $Mn^{2+}{}_B$, which is too far for an inner-sphere metal coordination interaction. However, the C232 C_α-C_β-Sγ → $Mn^{2+}{}_B$ dihedral angle is 170°, which reflects a nearly optimal, trans-oriented cysteine → metal coordination interaction (*26*). Although cysteine is not a common ligand to Mn^{2+} in biological systems, the cysteine thiolate can nonetheless stabilize Mn^{2+} binding through inner- or outer-sphere interactions. A search of the Metalloprotein Database and Browser (*27*) shows that three protein structures contain cysteine or methionine S → Mn^{2+} interactions with separations of 2.6−3.1 Å: 3-deoxy-D-arabino-heptulosanate-7-phosphate synthase (*28*), β1,4-galactosyltransferase (*29*), and lactose synthase (*30*). A search of S → Mn^{2+} interactions

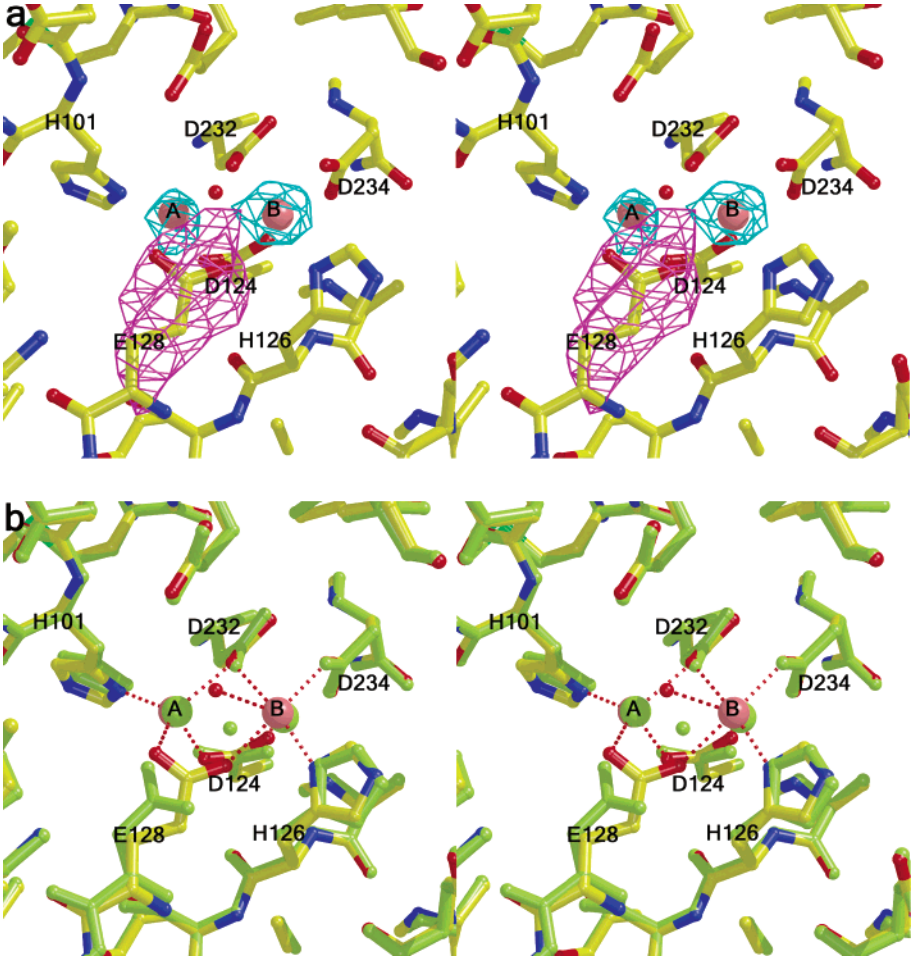

FIGURE 3: D128E arginase I. (a) Simulated annealing omit electron density maps of the binuclear manganese cluster calculated with Fourier coefficients $|F_o| - |F_c|$ less the atoms of E128 (magenta, contoured at 4.2σ) or Mn^{2+}_A and Mn^{2+}_B (cyan, contoured at 8.2σ). (b) Manganese coordination interactions (red dashed lines). For reference, the native arginase I structure is superimposed (pale green).

with separations of 1.9−3.0 Å in the Cambridge Structural Database (*31*) retrieves 124 examples, 20 of which have lengthier separations of 2.5−3.0 Å. Therefore, outer-sphere S → Mn^{2+} interactions occur with some frequency, and although weak, we conclude that the 3.0 Å C232 thiolate → Mn^{2+}_B interaction contributes to the retention of Mn^{2+}_B in the D232C variant with 70% occupancy. This contrasts with the complete loss of Mn^{2+}_B in the D232A variant, in which of course metal coordination by A232 is impossible.

Kinetic measurements made with D232 variants are consistent with the postulate that an intact binuclear manganese cluster is required for catalytic activity. In D232A arginase I, the loss of Mn^{2+}_B essentially abolishes activity (Table 3). The D232 carboxylate is required to stabilize Mn^{2+}_B and the metal-bridging hydroxide ion in their proper positions for catalysis. The near-obliteration of activity in this variant conclusively demonstrates that an intact binuclear manganese cluster is required for optimal catalysis.

In D232C arginase I, the binuclear manganese cluster remains largely intact because of the substitution of a different, although imperfect, ligand to Mn^{2+}_B. Very modest catalytic activity is retained in this variant: the k_{cat}/K_M value of 1.5 mM^{-1} s^{-1} is 0.8% of that measured for the wild-type enzyme (Table 3). The proper positioning of the nucleophilic hydroxide ion is affected by the D232C substitution even though it is not visible in the relatively low resolution electron density maps of Figure 2. An altered hydroxide position presumably accounts for the 120-fold lower k_{cat}/K_M value for this variant relative to that of the wild-type enzyme.

Structural and Functional Consequences of D128 Substitutions. The side chain of D128 plays a dual role in the binuclear manganese cluster: Oδ1 coordinates to Mn^{2+}_A, and Oδ2 accepts a hydrogen bond from the metal-bridging hydroxide ion in the native enzyme (Figure 1) (*4*) and from the metal-bridging hydroxyl groups of boronic acid analogues of the tetrahedral intermediate (*6*, *7*, *11*). Accordingly, Oδ2 of D128 is precisely positioned to interact with the nucleophilic hydroxide ion, and it may also mediate the proton transfer required for the collapse of the tetrahedral intermediate (*4*).

In D128E arginase I, the carboxylate functionality is preserved, but it is on a longer side chain. The binuclear manganese cluster is intact in this variant: Mn^{2+}_A is coordinated by E128 (Oϵ1), D124 (Oδ1), H101 (Nδ1), and D232 (Oδ1); and Mn^{2+}_B is coordinated by H126 (Nδ1), E128 (Oϵ2), D232 (Oδ1), D234 (Oδ2), D124 (Oδ2), and a solvent molecule; the Mn^{2+}_A−Mn^{2+}_B separation is 3.4 Å (Figure 3a), and the occupancy of Mn^{2+}_A refines to 80%.

Two subtle structural changes accompany the D128E substitution (Figure 3b). First, the side chain of E128 moves to bridge Mn^{2+}_A and Mn^{2+}_B through a somewhat-distorted, syn,syn bidentate interaction. The interaction with E128 may contribute to the 0.6 Å shift of Mn^{2+}_B toward the substituted side chain; there is no significant movement of Mn^{2+}_A.

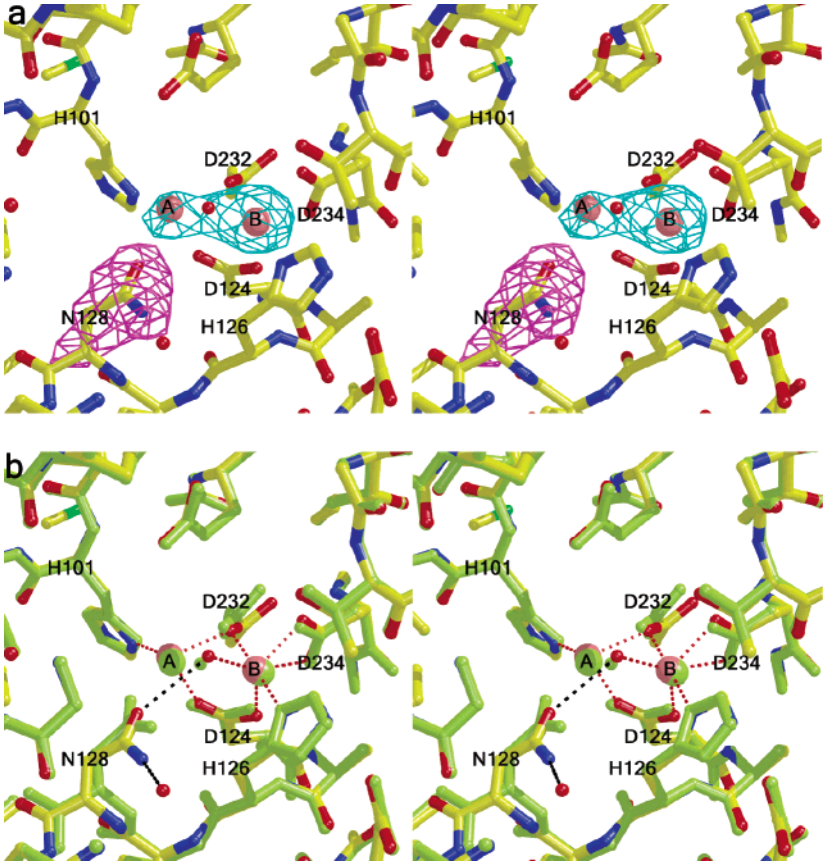

FIGURE 4: D128N arginase I. (a) Simulated annealing omit electron density maps of the binuclear manganese cluster calculated with Fourier coefficients $|F_o| - |F_c|$ less the atoms of N128 (magenta, contoured at 3.8σ) or Mn^{2+}_A and Mn^{2+}_B (cyan, contoured at 7.8σ). (b) Manganese coordination and solvent hydrogen bond interactions (red and black dashed lines, respectively). For reference, the native arginase I structure is superimposed (pale green).

Additionally, D234 changes from symmetrically bidentate to monodentate coordination with Mn^{2+}_B. The metal-bridging solvent molecule observed in the native enzyme moves 1.4 Å away from its original position to avoid a steric clash with Oϵ2 of E128.

In D128N arginase I, the substituted carboxamide side chain is isosteric with the wild-type carboxylate chain, and it potentially preserves an Oδ atom for Mn^{2+}_A coordination. However, Mn^{2+}_A is coordinated only by D124 (Oδ1), H101 (Nδ1), and D232 (Oδ1); with an O$-Mn^{2+}_A$ separation of 3.1 Å, N128 does not make an inner-sphere coordination interaction (Figure 4a). The Mn^{2+}_B ion is coordinated by H126 (Nδ1), D234 (Oδ1 and Oδ2), D232 (Oδ1), D124 (Oδ2), and a solvent molecule; the average $Mn^{2+}_A - Mn^{2+}_B$ separation is 3.4 Å. The Mn^{2+}_A ion refines with 50% occupancy, suggesting that the loss of a strong coordination interaction with D128 weakens metal affinity in the A site. Subtle structural changes accompany the D128N substitution: the side chain of N128 undergoes a 31° conformational change about χ_2, the N128 backbone atoms shift ~0.9 Å, and a solvent molecule hydrogen bonds to the Nδ atom of N128 (Figure 4b). The formerly metal-bridging solvent molecule moves 0.6 Å to coordinate exclusively to Mn^{2+}_B.

The structural consequences of D128N substitutions severely compromise the function of this residue in Mn^{2+}_A coordination as well as its function in hydrogen bonding to metal-bridging hydroxyl groups. Accordingly, it is not surprising that D128 substitutions dramatically compromise catalysis (Table 3). Consider D128E arginase I: although a binuclear manganese cluster is preserved in nearly the exact location as observed in the native enzyme, the longer E128 side chain extends further into the active site and coordinates to both Mn^{2+}_A and Mn^{2+}_B. In turn, the former metal-bridging hydroxide ion shifts 2.6 Å to coordinate exclusively to Mn^{2+}_B (Figure 3). The loss of the strategic positioning of the nucleophilic hydroxide ion is responsible for the 3600-fold decrease in k_{cat}/K_M for this variant.

Catalytic activity is even lower in D128N arginase I, with k_{cat}/K_M reduced 60 000-fold relative to the wild-type enzyme (Table 3). The crystal structure of this variant reveals that the engineered N128 side chain does not even coordinate to Mn^{2+}_A, resulting in only 50% occupancy for Mn^{2+}_A. This suggests that an asparagine$-Mn^{2+}_A$ coordination interaction is an inappropriate substitution for the wild-type aspartate$-Mn^{2+}_A$ interaction. Moreover, if the D128N substitution were to be perfectly isosteric, with Oδ of N128 coordinating to Mn^{2+}_A, the metal-bridging hydroxide ion would have to accept a hydrogen bond from N128. With the polarity of this hydrogen bond reversed, the nucleophilic lone electron pair of the hydroxide ion would be engaged in this hydrogen bond and therefore unavailable for catalysis.

Notably, catalytic activity is similarly compromised for the D128A variant (Table 3). Although this variant did not yield suitable crystals for X-ray diffraction analysis, by analogy with the D128N variant we conclude that the massive catalytic loss arises from weakened Mn^{2+}_A binding and the loss of a critical hydrogen bond interaction with metal-bridging hydroxyl groups.

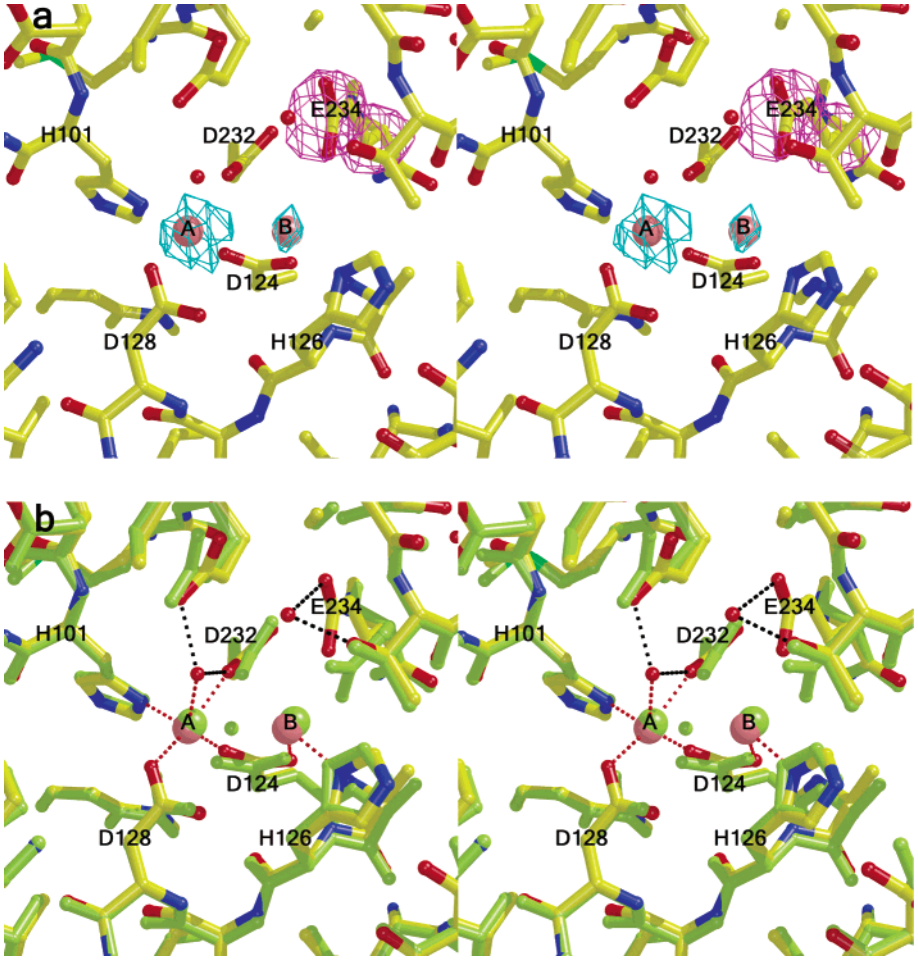

FIGURE 5: D234E arginase I. (a) Simulated annealing omit electron density maps of the binuclear manganese cluster calculated with Fourier coefficients $|F_o| - |F_c|$ less the atoms of E234 (magenta, contoured at 4.2σ) or Mn^{2+}_A and Mn^{2+}_B (cyan, contoured at 9.4σ). (b) Manganese coordination and solvent hydrogen bonding interactions (red and black dashed lines, respectively). For reference, the native arginase I structure is superimposed (pale green).

Structural and Functional Consequences of D234 Substitutions. In the wild-type enzyme, D234 makes a symmetric bidentate coordination interaction with Mn^{2+}_B. In the D234E variant, the carboxylate side chain moves away from metal coordination even though it is one methylene group longer than the wild-type side chain (Figure 5a). Mn^{2+}_A is coordinated by D124 (Oδ1), D128 (Oδ1), H101(Nδ1), D232 (Oδ2), and a solvent molecule, while Mn^{2+}_B is coordinated by D124 (Oδ2), H126 (Nδ1), and D232 (Oδ2); the Mn^{2+}_A−Mn^{2+}_B separation is 3.3 Å, and Mn^{2+}_B refines with 50% occupancy.

The E234 Oϵ1−Mn^{2+}_B separation is 2.8 Å, which is too long for inner-sphere metal coordination and accordingly weakens metal affinity in the B site. Interestingly, the metal pair shifts 0.2−0.3 Å away from the E234 side chain (Figure 5b). The formerly metal-bridging solvent molecule moves 1.6 Å closer to E277 and D232 and coordinates exclusively to Mn^{2+}_A (Figure 5b). The E234 side chain moves into the position formerly occupied by water molecule #22 of the native structure. The Oϵ2 atom of D234E accepts a hydrogen bond from the backbone NH group of T246 and a solvent molecule.

Among the three variants studied—D234E, D234A, and D234H arginases I—the D234E variant retains the most catalytic activity, although k_{cat}/K_M is reduced 69-fold as compared with the wild-type enzyme (Table 3). Unfortunately, we were unable to prepare suitable crystals of D234A and D234H arginases I for X-ray diffraction analysis, but it is reasonable to conclude that these variants undergo even more extensive structural perturbations in their manganese coordination polyhedra than those observed in D234E arginase I.

Structural and Functional Consequences of H101 Substitutions. In the wild-type enzyme, H101 coordinates to Mn^{2+}_A and donates a hydrogen bond to the S230 hydroxyl group, which in turns donates a hydrogen bond to the carboxylate of D274. This hydrogen bond network likely modulates the ability of Mn^{2+}_A to polarize the metal-bridging solvent molecule, just as carboxylate−histidine interactions help to modulate the basicity of the zinc-bound solvent molecule in carbonic anhydrase II (*32*−*34*). The structural and functional consequences of the H101E substitution are potentially severe, then: not only is a nonisosteric and negatively charged glutamate side chain substituted for the neutral imidazole ligand to Mn^{2+}_A (i.e., Oϵ^- → Mn^{2+}_A coordination replaces Nδ → Mn^{2+}_A coordination), but the hydrogen bond network with H101 is disrupted since E101 cannot donate a hydrogen bond to S230.

Surprisingly, H101E arginase I exhibits the second-highest level of residual catalytic activity of all variants studied (Table 3). The crystal structure of the H101E arginase I−BEC complex reveals that the E101 Oϵ^- → Mn^{2+}_A

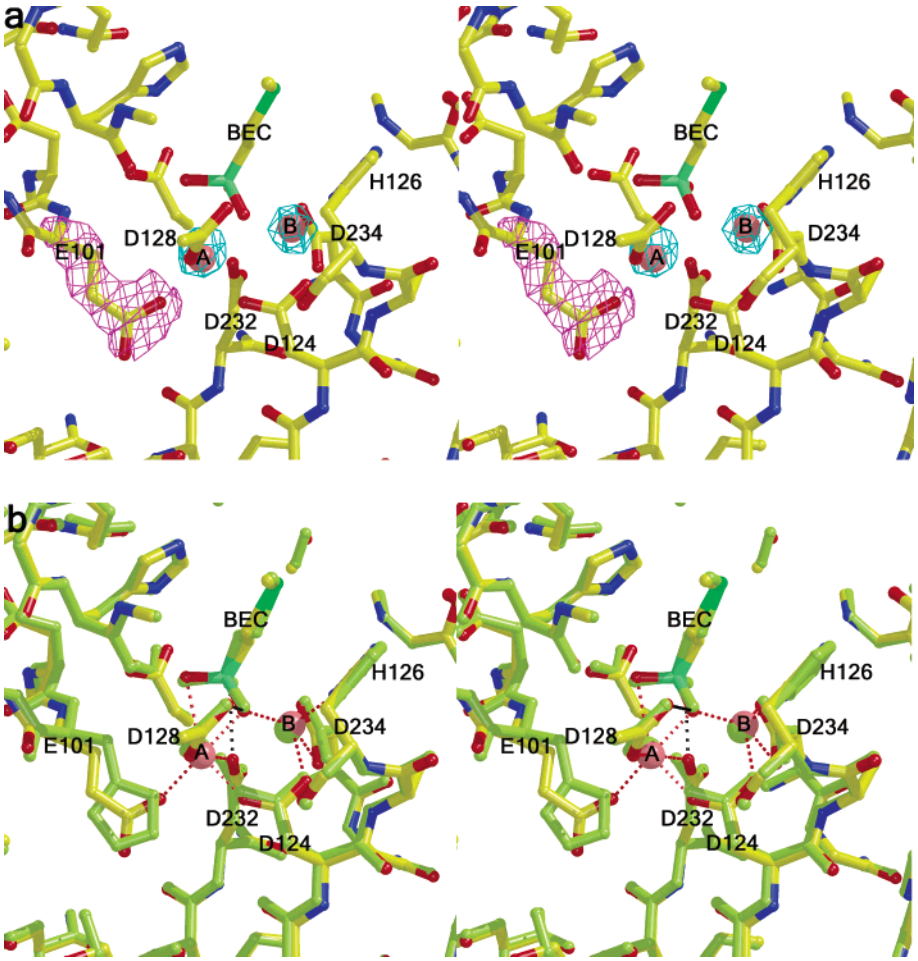

FIGURE 6: H101E-BEC arginase I complex. (a) Simulated annealing omit electron density maps of the binuclear manganese cluster calculated with Fourier coefficients $|F_o| - |F_c|$ less the atoms of E101 (magenta, contoured at 3σ) or Mn^{2+}_A and Mn^{2+}_B (cyan, contoured at 9.1σ). (b) Manganese coordination and solvent and BEC hydrogen bond interactions (red and black dashed lines, respectively). For reference, the native arginase I structure is superimposed (pale green).

coordination interaction is almost exactly superimposable on the wild-type H101 N$\delta \rightarrow Mn^{2+}_A$ interaction, and the metal-bridging hydroxyl group of BEC is similarly positioned in both complexes (*7*) (Figure 6). Thus, the positions of the binuclear manganese cluster and the metal-bridging hydroxyl group are perturbed very little in this variant, and this accounts for significant residual activity.

In the H101E arginase I−BEC complex, Mn^{2+}_A is coordinated by E101 (Oϵ1), D128 (Oδ1), D232 (Oδ2), D124 (Oδ1), and boronate hydroxyl groups O1 and O2; Mn^{2+}_B is coordinated by H126 (Nδ1), D124 (Oδ1), D234 (Oδ1 and Oδ2), and boronate hydroxyl group O1; the Mn^{2+}_A−Mn^{2+}_B separation is 3.6 Å, and both metals are bound with full occupancy. Boronate hydroxyl group O1 symmetrically bridges the binuclear manganese cluster and donates a hydrogen bond to the Oδ2 of D128. Boronate hydroxyl group O2 coordinates to Mn^{2+}_A and also donates a hydrogen bond to the backbone carbonyl group of H141. Boronate hydroxyl group O3 donates a hydrogen bond to D232 (Oδ2). The main structural difference between H101E and native arginase I is the loss of the H101−S230 hydrogen bond. The loss of this interaction appears to cause a 100° rotation around the χ_1 torsion angle of S230, which allows it to retain its hydrogen bond with D274.

H101N arginase I exhibits the highest residual catalytic activity of any metal-site variant studied, with k_{cat}/K_M reduced only 1.5-fold relative to the wild-type enzyme (Table 3) (*9*). The crystal structure of this variant reveals a binuclear manganese cluster (Mn^{2+}_A and Mn^{2+}_B having occupancies of 50 and 100%, respectively) with metal ion positions only slightly changed from those of the wild-type enzyme (Figure 7). Further refinement of the metal-loaded H101N arginase I structure reported by Scolnick and co-workers at 2.5 Å resolution (*10*) (PDB 3RLA) reveals that the Oδ of N101 coordinates to Mn^{2+}_A ($R_{cryst} = 0.237$, $R_{free} = 0.263$; rms deviations: 0.009 Å (bonds), 1.3° (angles)). The side chain NH_2 group of N101 hydrogen bonds to a solvent molecule, which in turn hydrogen bonds to S230. Accordingly, the hydrogen bond interaction between S230 and D274 is not obliterated as it is in the H101E variant, but it is instead mediated by a solvent molecule (Figure 7). This may account for the substantial residual activity of H101N arginase I.

CONCLUSION

The current work represents the first detailed molecular dissection of the binuclear manganese cluster of arginase I using site-directed mutagenesis and X-ray crystallography, and as such, this work provides valuable structural inferences on the role of the metal cluster in catalysis. Additionally, this work serves as a paradigm for understanding structure−function and structure−stability relationships in other binuclear metalloenzymes.

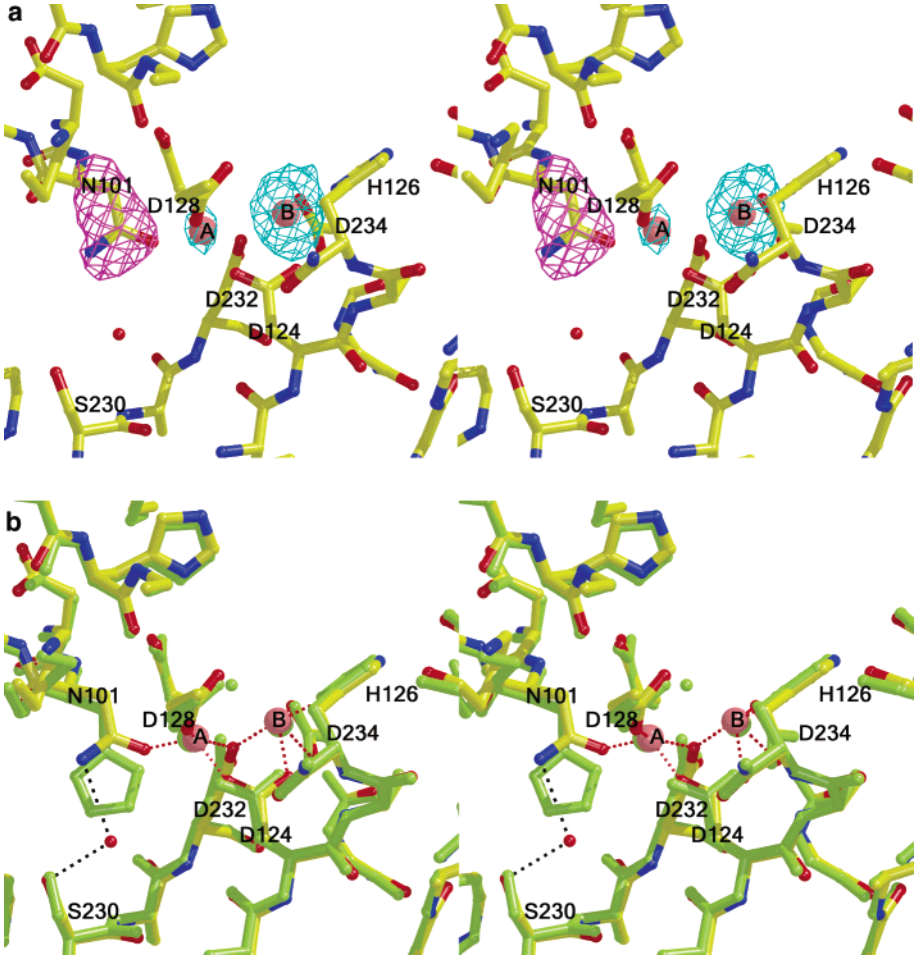

FIGURE 7: H101N arginase I. (a) Simulated annealing omit electron density maps of the binuclear manganese cluster calculated with Fourier coefficients $|F_o| - |F_c|$ less the atoms of N101 (magenta, contoured at 3.7σ) or Mn^{2+}_A and Mn^{2+}_B (cyan, contoured at 9.6σ). (b) Manganese coordination and solvent hydrogen bond interactions (red and black dashed lines, respectively). For reference, the native arginase I structure is superimposed (pale green).

Amino acid substitutions in the first shell metal ligands compromise catalytic activity over 5 orders of magnitude on k_{cat} (Table 3). The structural basis for activity loss is the disruption of the metal cluster and the nucleophilic metal-bridging hydroxide ion by (a) shifting the position(s) of one or both metal ions, (b) weakening the binding of either Mn^{2+}_A or Mn^{2+}_B so as to increase the population of inactive mononuclear manganese sites, and/or (c) altering the net charge of the metal coordination polyhedra.

Variants that exhibit the highest level of residual activity (H101E, H101N) contain structurally intact metal clusters, and a structurally intact cluster contains a structurally intact metal-bridging hydroxide ion for catalysis. Moreover, a structurally intact metal cluster will bind and stabilize the tetrahedral intermediate and its flanking transition states, and this is manifest in the structural similarities in transition state analogue binding between wild-type and H101E arginases (Figure 6). That the H101E variant is ~45-fold less active than the H101N variant may be due to the introduction of an additional negative charge in the Mn^{2+}_A coordination polyhedron, thereby attenuating the ability of Mn^{2+}_A to activate the metal-bridging hydroxide ion for catalysis. Comparable structure activity relationships have been described for the mononuclear Zn^{2+} site of carbonic anhydrase II (*35*), and the current work demonstrates that such relationships also hold for Mn^{2+}−Mn^{2+} clusters.

Variants that exhibit the least residual catalytic activity (D128E, D128N, D128A) contain binuclear manganese clusters compromised by weakened binding of Mn^{2+}_A, resulting in lower Mn^{2+}_A occupancy. The crystal structures of the D128E and D128N variants additionally reveal that the positions of the metal ions and the metal-bound solvent molecules are significantly shifted (Figures 3 and 4). Moreover, neither variant is capable of stabilizing the metal-bound solvent molecule or the corresponding hydroxyl group of the tetrahedral intermediate and its flanking transition state by hydrogen bonding with the residue 128 side chain.

In summary, we conclude that the binuclear manganese cluster of arginase I evolved with the optimal structure and chemical properties to orient and activate the metal-bridging hydroxide ion for nucleophilic attack at substrate L-arginine. That the substrate K_M value remains relatively invariant despite the various disruptions of the metal cluster described in this work suggests that L-arginine is bound to a nonmetal site prior to nucleophilic attack. As predicted by Kanyo and co-workers (*4*) and verified in the binding of the substrate to the Mn^{2+}_B-depleted *Bacillus caldovelox* arginase (*36*), and as verified in the binding of tetrahedral transition state analogues to rat arginase I (*6*, *7*) and human arginase II (*11*), the nonmetal substrate binding site is a salt-link with the negatively charged side chain of E277 and a hydrogen bond with the backbone carbonyl of H141.

ACKNOWLEDGMENT

We thank the Stanford Synchrotron Radiation Laboratory and the Cornell High Energy Synchrotron Source for access to X-ray diffraction data collection facilities.

REFERENCES

1. Christianson, D. W., and Cox, J. D. (1999) *Annu. Rev. Biochem. 68*, 33−57.
2. Ash, D. E., Cox, J. D., and Christianson, D. W. (2000) in *Manganese and its Role in Biological Processes*, Vol. 37 of *Metal Ions in Biological Systems* (Sigel, A. and Sigel, H., Eds.) p 408−428, M. Dekker, New York.
3. Morris, S. M., Jr. (2002) *Annu. Rev. Nutr. 22*, 87−105.
4. Kanyo, Z. F., Scolnick, L. R., Ash, D. E., and Christianson, D. W. (1996) *Nature 383*, 554−557.
5. Reczkowski, R. S., and Ash, D. E. (1992) *J. Am. Chem. Soc. 114*, 10992−10994.
6. Cox, J. D., Kim, N. N., Traish., A. M., and Christianson, D. W. (1999) *Nat. Struct. Biol. 6*, 1043−1047.
7. Kim, N. N., Cox, J. D., Baggio, R. F., Emig, F. A., Mistry, S., Harper, S. L., Speicher, D. W., Morris, S. M., Ash, D. E., Traish, A. M., and Christianson, D. W. (2001) *Biochemistry 40*, 2678−2688.
8. Khangulov, S. V., Sossong, T. M., Jr., Ash, D. E., and Dismukes, G. C. (1998) *Biochemistry 37*, 8539−8550.
9. Cavalli, R. C., Burke, C. J., Kawamoto, S., Soprano, D. R., and Ash, D. E. (1994) *Biochemistry 33*, 10652−10657.
10. Scolnick, L. R., Kanyo, Z. F., Cavalli, C. R., Ash, D. E., and Christianson, D. W. (1997) *Biochemistry 36*, 10558−10565.
11. Cama, E., Colleluori, D. M., Emig, F. A., Shin, H., Kim, S. W., Kim, N. N., Traish, A. M., Ash, D. E., and Christianson, D. W. (2003) *Biochemistry*, in press.
12. Rüegg, U. T., and Russell, A. S. (1980) *Anal. Biochem. 102*, 206−212.
13. Wilson, A. J. C. (1950) *Acta Crystallogr. 3*, 397−398.
14. Stanley, E. (1972) *J. Appl. Cryst. 5*, 191.
15. Yeates, T. O. (1997) *Methods Enzymol. 276*, 344−358.
16. Redinbo, M. R., and Yeates, T. O. (1993) *Acta Crystallogr. D49*, 375−380.
17. Otwinowski, Z., and Minor, W. (1997) *Methods Enzymol. 276*, 307−326.
18. Brünger, A. T., Adams, P. D., Clore, G. M., DeLano, W. L., Gros, P., Grosse-Kunstleve, R. W., Jiang, J. S., Kuszewski, J., Nilges, M., Pannu, N. S., Read, R. J., Rice, L. M., Simonson, T., and Warren, G. L. (1998) *Acta Crystallogr. D54*, 905−921.
19. Jones, T. A., Zou, J.-Y., Cowan, S. W., and Kjeldgaard, M. (1991) *Acta Crystallogr. A47*, 110−119.
20. Navaza, J. (1994) *Acta Crystallogr. A50*, 157−163.
21. Collaborative Computational Project, No. 4. (1994) *Acta Crystallogr. D50*, 760−763.
22. Esnouf, R. M. (1997) *J. Mol. Graphics 15*, 132−134.
23. Merritt, E. A., and Bacon, D. J. (1997) *Methods Enzymol. 277*, 505−524.
24. Chaberek, S., Jr., Courtney, R. C., and Martell, A. E. (1952) *J. Am. Chem. Soc. 74*, 5057−5060.
25. Kuhn, N. J., Talbot, J., and Ward, S. (1991) *Arch. Biochem. Biophys. 286*, 217−221.
26. Chakrabarti, P. (1989) *Biochemistry 28*, 6081−6085.
27. Castagnetto, J. M., Hennessy, S. W., Roberts, V. A., Getzoff, E. D., Tainer, J. A., and Pique, M. E. (2002) *Nucleic Acids Res. 30*, 379−382.
28. Shumilin, I. A., Zhao, C., Bauerle, R., and Kretsinger, R. H. (2002) *J. Mol. Biol. 320*, 1147−1156.
29. Ramakrishnan, B., and Qasba, P. K. (2002) *J. Biol. Chem. 277*, 20833−20839.
30. Ramakrishnan, B., and Qasba, P. K. (2001) *J. Mol. Biol. 310*, 205−218.
31. Allen, F. H., Kennard, O., and Taylor, R. (1983) *Acc. Chem. Res. 16*, 146−153.
32. Kiefer, L. L., Paterno, S. A., and Fierke, C. A. (1995) *J. Am. Chem. Soc. 117*, 6831−6837.
33. Lesburg, C. A., and Christianson, D. W. (1995) *J. Am. Chem. Soc. 117*, 6838−6844.
34. Christianson, D. W., and Alexander, R. S. (1989) *J. Am. Chem. Soc. 111*, 6412−6419.
35. Christianson, D. W., and Fierke, C. A. (1996) *Acc. Chem. Res. 29*, 331−339.
36. Bewley, M. C., Jeffrey, P. D., Patchett, M. L., Kanyo, Z. F., and Baker, E. N. (1999) *Structure 7*, 435−448.

BI030074Y